AFRL-PR-WP-TP-2006-203

ADDITION OF ALTERNATE PHASE NANOPARTICLE DISPERSIONS TO ENHANCE FLUX PINNING OF Y-Ba-Cu-O THIN FILMS

Timothy J. Haugan, Paul N. Barnes, Timothy A. Campbell, Julianna M. Evans, Joseph W. Kell, Lyle B. Brunke, John P. Murphy, Chakrapani Varanasi, Iman Maartense, Winnie Wong-Ng, and Lawrence P. Cook

OCTOBER 2004

Approved for public release; distribution is unlimited.

STINFO COPY

PROPULSION DIRECTORATE
AIR FORCE MATERIEL COMMAND
AIR FORCE RESEARCH LABORATORY
WRIGHT-PATTERSON AIR FORCE BASE, OH 45433-7251

REPORT DOCUMENTATION PAGE

Form Approved
OMB No. 0704-0188

1. REPORT DATE *(DD-MM-YY)*	2. REPORT TYPE	3. DATES COVERED *(From - To)*
October 2004	Journal Article Postprint	10/05/2003 – 10/05/2004

4. TITLE AND SUBTITLE
ADDITION OF ALTERNATE PHASE NANOPARTICLE DISPERSIONS TO ENHANCE FLUX PINNING OF Y-Ba-Cu-O THIN FILMS

5a. CONTRACT NUMBER
In-house

5b. GRANT NUMBER

5c. PROGRAM ELEMENT NUMBER
61102F/62203F

6. AUTHOR(S)
Timothy J. Haugan, Paul N. Barnes, Timothy A. Campbell, Julianna M. Evans, Joseph W. Kell, Lyle B. Brunke, John P. Murphy, Chakrapani Varanasi, Iman Maartense, Winnie Wong-Ng, and Lawrence P. Cook

5d. PROJECT NUMBER
3145

5e. TASK NUMBER
32

5f. WORK UNIT NUMBER
31453279

7. PERFORMING ORGANIZATION NAME(S) AND ADDRESS(ES)
Power Generation Branch (AFRL/PRPG)
Power Division
Propulsion Directorate
Air Force Research Laboratory, Air Force Materiel Command
Wright-Patterson Air Force Base, OH 45433-7251

8. PERFORMING ORGANIZATION REPORT NUMBER
AFRL-PR-WP-TP-2006-203

9. SPONSORING/MONITORING AGENCY NAME(S) AND ADDRESS(ES)
Propulsion Directorate
Air Force Research Laboratory
Air Force Materiel Command
Wright-Patterson AFB, OH 45433-7251

10. SPONSORING/MONITORING AGENCY ACRONYM(S)
AFRL-PR-WP

11. SPONSORING/MONITORING AGENCY REPORT NUMBER(S)
AFRL-PR-WP-TP-2006-203

12. DISTRIBUTION/AVAILABILITY STATEMENT
Approved for public release; distribution is unlimited.

13. SUPPLEMENTARY NOTES
Journal article postprint published in IEEE Transactions on Applied Superconductivity, Vol. 15, No. 2, June 2005.

PAO case number: AFRL/WS 05-0210; Date cleared: 04 Feb 2005. Paper contains color.

14. ABSTRACT
Nanoparticle dispersions of various phases were added to $YBa_2Cu_3O_{7-x}$ (YBCO or 123) thin films by multilayer pulsed laser deposition, to determine their effect on flux pinning. The different pinning materials examined include Y_2BaCuO_5 (Y211 or green-phase), La_2BaCuO_5 (La211 or brown-phase), Y_2O_3, CeO_2, and MgO, with lattice constant mismatches varying from 0.5% to 12% with respect to YBCO. Y211 and Y_2O_3 provided significant pinning increases at temperatures of 65 K and 77 K, however other phases provided enhancements only at 65 K (for CeO_2 and La211) for limited range of applied field strengths. An interesting correlation between T_c transition widths and pinning strengths was observed. The additions produced markedly different nanoparticle and film microstructures,as well as superconducting properties.

15. SUBJECT TERMS
flux pinning, high temperature superconductor, nanoparticle, $YBa_2Cu_3O_{7-x}$, thin film

16. SECURITY CLASSIFICATION OF:			17. LIMITATION OF ABSTRACT:	18. NUMBER OF PAGES	19a. NAME OF RESPONSIBLE PERSON (Monitor)
a. REPORT	b. ABSTRACT	c. THIS PAGE			Paul N. Barnes
Unclassified	Unclassified	Unclassified	SAR	10	19b. TELEPHONE NUMBER *(Include Area Code)* N/A

Addition of Alternate Phase Nanoparticle Dispersions to Enhance Flux Pinning of Y-Ba-Cu-O Thin Films

Timothy J. Haugan, *Member, IEEE*, Paul N. Barnes, Timothy A. Campbell, Julianna M. Evans, Joseph W. Kell, Lyle B. Brunke, John P. Murphy, Chakrapani Varanasi, Iman Maartense, Winnie Wong-Ng, and Lawrence P. Cook

***Abstract*—Nanoparticle dispersions of various phases were added to $YBa_2Cu_3O_{7-x}$ (YBCO or 123) thin films by multilayer pulsed laser deposition, to determine their effect on flux pinning. The different pinning materials examined include Y_2BaCuO_5 (Y211 or green-phase), La_2BaCuO_5 (La211 or brown-phase), Y_2O_3, CeO_2, and MgO, with lattice constant mismatches varying from 0.5% to 12% with respect to YBCO. Y211 and Y_2O_3 provided significant pinning increases at temperatures of 65 K and 77 K, however other phases provided enhancements only at 65 K (for CeO_2 and La211) for limited range of applied field strengths. An interesting correlation between T_c transition widths and pinning strengths was observed. The additions produced markedly different nanoparticle and film microstructures, as well as superconducting properties.**

***Index Terms*—Flux pinning, high temperature superconductor, nanoparticle, $YBa_2Cu_3O_{7-x}$ thin film.**

I. Introduction

THE DEVELOPMENT of high temperature superconductor $YBa_2Cu_3O_{7-\delta}$ (YBCO or 123) thin films on polycrystalline substrates (coated conductors) with a critical current density $(J_c) > 1\ MA/cm^2$ offers great promise for incorporation into power applications such as generators or motors, operating at 77 K [1]–[5]. YBCO has excellent properties at 77 K including high $J_c(H)$ due to strong flux pinning. However it is of interest to increase $J_c(H)$ even further to increase wire performance and reduce production costs [1], [2]. For type-II superconductors, it is known that flux pinning can be increased by incorporating a high density of extended non-superconducting defects into the material [2]–[4]. The defect size should be approximately the coherence length ~(2–4) nm at (4.2–77) K to maximize pinning [2]–[4].

Previously, we have added near-uniform dispersions of nano-size particles to YBCO by deposition of $(X/123) \times N$ multilayer films (X = Y211, Y_2O_3 or CeO_2 = 0.2 – 2.0 nm thick, 123 = 10 – 30 nm thick) [6]–[11]. With this deposition method nanoparticles form by the island-growth mechanism and can be coherently embedded in a superlattice-type structure with sizes as small as ~8 nm, and areic number densities estimated $> 4 \times 10^{11}\ particles/cm^2$ [6]. Significant increases of transport $J_c(H)$ up to 3x were measured at 77 K for additions of Y211 nanoparticles [6]. This and similar experiments with $BaZrO_3$ + YBCO films demonstrate that dispersions of point-like defects can significantly increase flux pinning [5], [6]. Despite these recent experimental results, there are many questions remaining concerning the flux pinning mechanisms and how point-defects can be implemented in YBCO. Some of the questions include what is the maximum $J_c(H)$ that can be achieved, what types of nanoparticles are effective, are there stress or lower T_c regions surrounding the nanoparticles that assist in pinning, what is the relation between volumic or areic number densities to pinning strengths, and others.

In this paper, general questions about dispersion pinning are explored by comparing multilayer deposition of different pinning materials, including Y211, Y_2O_3, CeO_2 MgO, and La211. La211 and Nd211 are referred to as 'brown-phase' because of their color, compared to other rare-earth (RE) 211 compounds which are green [12]. Each of these phases has unique materials properties (Table I) that can affect the epitaxial growth and flux pinning enhancements. Other factors such as the chemical nature or compatibility of epitaxial bonding were not considered at this time. As will be concluded, the lattice mismatch and chemical compatibility of the phases are important factors that affect the film microstructure and superconducting properties.

TABLE I
PHYSICAL PROPERTIES OF PINNING AGENTS

Phase	Crystal Type	Lattice mismatch*	Nanoparticle Shape
Y_2BaCuO_5	tetragonal	+4% to – 7% **	hockey-puck
Y_2O_3	cubic	– 2.5% ***	
CeO_2	cubic	– 0.5% ***	monolayer
MgO	cubic	+ 9.6%	
La_2BaCuO_5	tetragonal	+5% to – 12%	

* Using lattice parameter of YBCO $(a,b)_{avg}$ = 3.845 Å.
** *b*-axis orientation predominant growth [6].
*** Lattice constant = a/(√2).

II. Experimental Procedures

Multilayer $(X - phase/123) \times N$ and 123-only films were deposited onto $LaAlO_3$ (LAO) and $SrTiO_3$ (STO) 100 oriented single crystal substrates by pulsed laser deposition (PLD), using parameters and conditions described in detail previously [6]–[12]. Deposition parameters were 248 nm laser wavelength, ~ 3.2 J/cm^2 laser fluence, 4 Hz laser repetition rate, 6 cm target-to-substrate distance, 780°C heater block temperature,

Manuscript received October 5, 2004. This work was supported in part by the U.S. Air Force Office of Scientific Research and the Air Force Research Laboratory.

T. J. Haugan, P. N. Barnes, T. A. Campbell, J. M. Evans, J. W. Kell, L. B. Brunke, J. P. Murphy, C. Varanasi, and I. Maartense are with the Air Force Research Laboratory, Wright-Patterson AFB, OH 45431 USA (e-mail: timothy.haugan@wpafb.af.mil).

W. Wong-Ng and L. P. Cook are with National Institute of Standards and Technology, Gaithersburg, MD 20899-8520 USA (e-mail: winnie.wong-ng@nist.gov).

Digital Object Identifier 10.1109/TASC.2005.849427

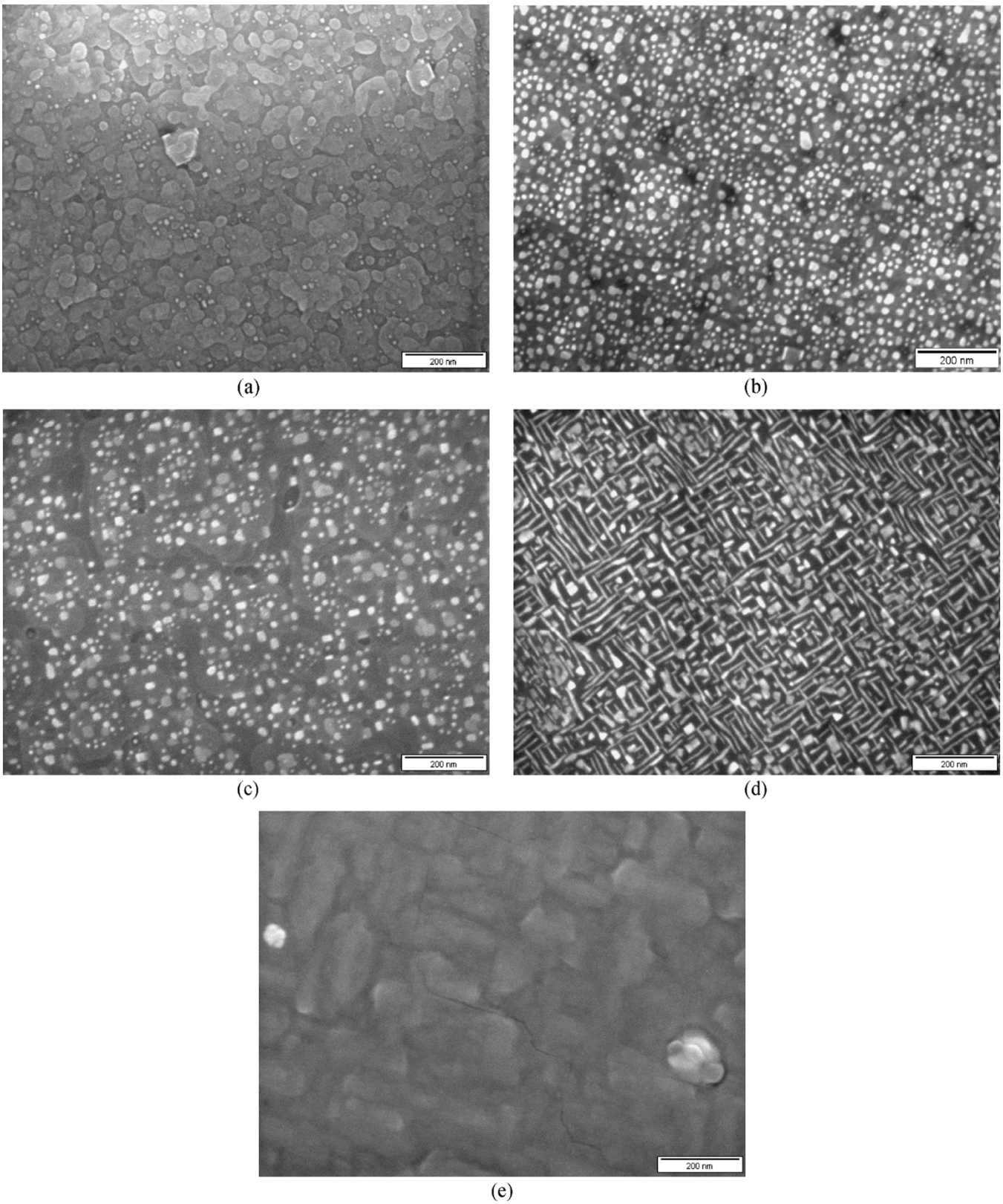

Fig. 1. Ultra-high resolution SEM micrographs at 100 000x magnification of $(\mathrm{X}/123) \times \mathrm{N}$ multilayer film surfaces. Insulating phases are (white or lighter) color from enhanced surface charging and emission of imaging electrons: (b) average particle size ∼13 nm, (c) average particle size ∼15 nm. (a) $(\mathrm{CeO}_{2\ 1.2\ \mathrm{nm}}/123_{15.6\ \mathrm{nm}}) \times 24/\mathrm{STO}$; (b) $(\mathrm{Y_2O_{3\ 1.36\ nm}}/123_{9.9\ \mathrm{nm}}) \times 28/\mathrm{STO}$; (c) $(\mathrm{Y211}_{1.2\ \mathrm{nm}}/123_{13.9\ \mathrm{nm}}) \times 25/\mathrm{STO}$; (d) $(\mathrm{MgO}_{1.2\ \mathrm{nm}}/123_{20\ \mathrm{nm}}) \times 19/\mathrm{STO}$; (e) $(\mathrm{La211}_{1.25\ \mathrm{nm}}/123_{11.9\ \mathrm{nm}}) \times 27/\mathrm{LAO}$.

(85–90)% dense targets, 300 mTorr oxygen partial-pressure, and a post-deposition anneal at 500°C and 1 atmosphere of oxygen [13]. For $\mathrm{CeO_2}$ depositions, the heater temperature was decreased to 750°C to reduce formation of ∼micron-sized defects presumed to be $\mathrm{BaCeO_3}$ from chemical reactions at 780°C heater temperature. An automated target rotation and

pulse-triggering system was used to control the deposition sequences, with a period of about 13 seconds during which the deposition was stopped and different targets were rotated into position. The deposition rate for each pinning material was calibrated prior to multilayer deposition. The 'pseudo-layer' thickness in the multilayer films was calculated assuming smooth continuous film coverage, although the layer in some cases consisted of discontinuous and discrete nanoparticles. The total film thickness was kept in the range of (250–350) nm to provide consistent comparisons, unless noted otherwise. The film thickness of every sample was measured multiple times across acid-etched step-edges with a profilometer (KLA-Tencor, P15), to obtain an average value.

The superconducting transition temperature (T_c) was measured using an AC susceptibility technique with the amplitude of the magnetic sensing field, h, varied from 0.025 Oe to 2.2 Oe, at a frequency of approximately 4 kHz. Note that the AC susceptibility technique provides information about primary and secondary transitions of the entire film, rather than a defined path that is obtained with transport T_c measurements. Magnetic J_c measurements were made with a vibrating sample magnetometer (VSM) in fields of 0 to 9 T, and a ramp rate of about 9,000 $(A/m \bullet s)$. The J_c of the square samples was estimated using a simplified Bean model $J_c = 15\Delta M/R$, where M is magnetization/volume from $M - H$ loops, and R is the radius of volume interaction = square side for consistency [7]. Characterization of microstructures was performed with scanning electron microscopy primarily in ultra-high resolution mode (SEM, FEI-Sirion).

III. Results

The effect of nanosize additions on the microstructural and superconducting properties are described in the following.

A. Microstructures

The microstructures of the film surfaces for the varying nanosize additions are shown in Fig. 1(a) to Fig. 1(e), in order of increasing lattice constant mismatch. The films showed unique features for each material system. A general trend was observed that as the lattice mismatch was increased from 0.5% to 7% (e.g. CeO_2 to Y211), the surface area coverage of the insulating phase decreased. While this trend is expected from island-formation nucleation mechanisms, other factors including chemical reactivity could affect the surface coverages. Cross-sectional TEM images of CeO_2 and Y211 films showed similar microstructures as SEM for the insulating phase; e.g. nearly monolayer flat ~50 nm-wide platelets for CeO_2 multilayer films, compared to 8-nm sized particles for Y211 multilayer films.

Film surfaces in Fig. 1 were also presumably affected by increased coalescence and ripening, as the top-layers were at temperatures $> 750°C$ typically about 10 minutes before subsequent cooling. Particle sizes for 211 were typically about 2 times larger diameter on the surface, than observed on the inside layers [6].

Some of the notable features in Fig. 1 were for MgO and La211 multilayer films which showed enhanced nano-rod and nanoparticle formation (MgO) or none at all (La211). For MgO the increased surface coverage for similar 'pseudo-layer' thickness suggests a chemical reaction is occurring, assuming the nano-rod particle heights are similar as for Y_2O_3 and Y211 nanoparticles. La211 multilayer films also showed signs of cracking throughout the film. Very wide T_c transitions for these materials were measured (Fig. 2) which strongly suggest there were chemical reactions occurring to reduce the T_c and disturb other microstructural properties.

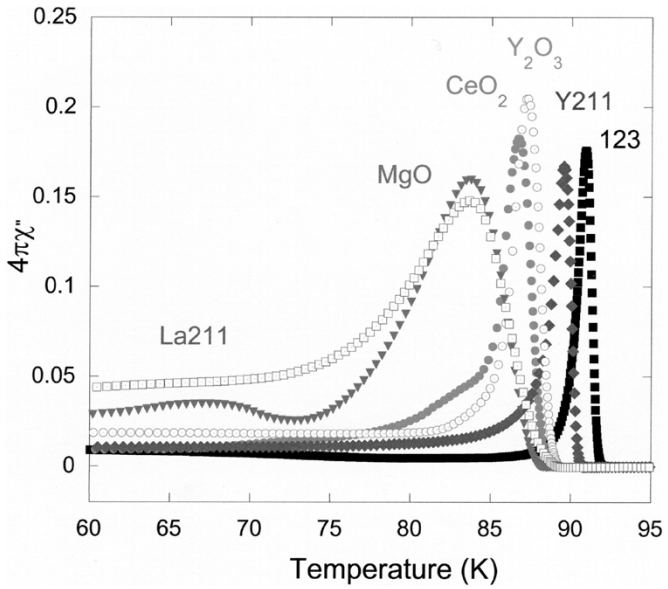

Fig. 2. Superconducting (χ'') transitions at 2.2 Oe for $(X/123) \times N$ multilayer films: $(Y211_{0.56\ nm}/123_{11.4\ nm}) \times 21/LAO$, $(Y_2O_{3,0.6\ nm}/123_{10\ nm}) \times 29/STO$, $(CeO_{2\ 0.24\ nm}/123_{16.3\ nm}) \times 25/STO$, $(La211_{1.2\ nm}/123_{11.7\ nm}) \times 27/LAO$, $(MgO_{1.0\ nm}/123_{20.4\ nm}) \times 19/STO$, and 123/LAO.

B. Superconducting Properties

The effect of nanosize additions on superconducting transitions are shown in Fig. 2. The transitions in Fig. 2 were representative of the $(X/123) \times N$ films, with the onsets and widths typically varying by about 1 K for similar samples.

Transition widths for Y_2O_3 and Y211 multilayer films were comparable to 123 films, and the onset temperatures were only slightly lower by about (1–2) K for low (3–5)% volume fraction additions (but decreased linearly with increasing volume fraction additions >5% [7], [11]). Transition onsets for CeO_2 multilayers (~89 K) did not show any decrease compared to 123-only films deposited on CeO_2 buffer layers, with T_c onsets ~(89–90)K which were repeatedly measured. This is consistent with the hypothesis that smaller lattice mismatched materials would exert less stress on the superconductor, and have less effect on T_c onsets.

A consistent trend in Fig. 2 is that the T_c transitions for high lattice mismatch materials (MgO and La211) were quite broad, with the loss transition not finished at 77 K. Films with superconducting transitions this wide always have very low J_cs at 77 K ranging anywhere from 100 A/cm^2 to 10^5 A/cm^2, from our experience. MgO also showed a second phase transition at temperature <70 K, indicating the film quality has been degraded.

The effect of nanosize additions on $J_c(H)$ properties are shown in Fig. 3. The $J_c(H)$ curves were representative of the highest measured thus far by optimizing the layer thickness parameters. Y211 and Y_2O_3 have consistently higher $J_c(H)$ curves compared to 123 at both 65 K and 77 K. The other

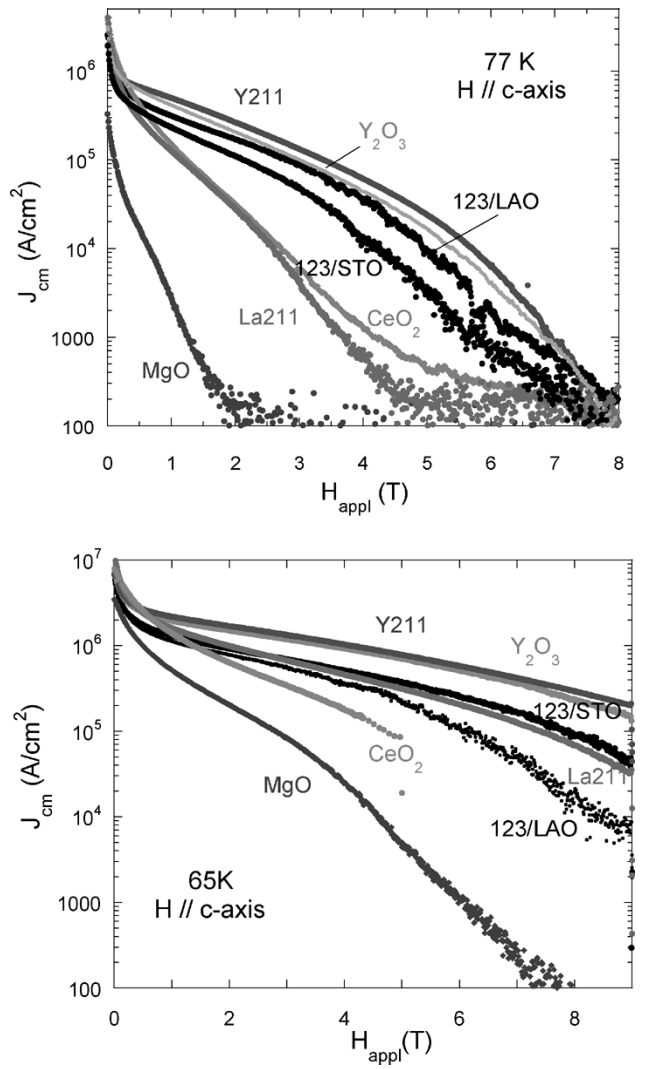

Fig. 3. Magnetic critical current density ($\mathrm{J_{cm}}$) as a function of applied field for $(\mathrm{X}/123) \times \mathrm{N}$ multilayer films at 77 K (upper): $(\mathrm{Y211_{0.8\ nm}}/\mathrm{123_{14.5\ nm}}) \times 13/\mathrm{LAO}$, $(\mathrm{Y_2O_{3\ 0.3\ nm}}/\mathrm{123_{47\ nm}}) \times 6/\mathrm{STO}$, $(\mathrm{CeO_{2,0.2\ nm}}/\mathrm{123_{12.8\ nm}}) \times 25/\mathrm{STO}$ from [10], $(\mathrm{La211_{1.7\ nm}}/\mathrm{123_{17.7\ nm}}) \times 15/\mathrm{LAO}$, $(\mathrm{MgO_{0.6\ nm}}/\mathrm{123_{20.4\ nm}}) \times 19/\mathrm{STO}$, and 123/LAO and 123/STO, and at 65 K (lower) same samples except films with slightly different parameters for $\mathrm{X} = \mathrm{Y211}$, $\mathrm{Y_2O_3}$ and $\mathrm{CeO_2}$: $(\mathrm{Y211_{1.0\ nm}}/\mathrm{123_{21.9\ nm}}) \times 13/\mathrm{LAO}$, $(\mathrm{Y_2O_{3,0.3\ nm}}/\mathrm{123_{86\ nm}}) \times 3/\mathrm{STO})$, and $(\mathrm{CeO_{2,0.3\ nm}}/\mathrm{123_{14.8\ nm}}) \times 25/\mathrm{STO}$ from [10].

pinning materials however exhibit varied pinning behaviors, especially comparing 65 K to 77 K. Also noteworthy is how 123/LAO has better properties than 123/STO at 77 K, but the order is reversed at 65 K.

IV. Discussions and Conclusions

For the $(\mathrm{X}/123) \times \mathrm{N}$ multilayers systems tested in this paper, only $\mathrm{X} = \mathrm{Y_2O_3}$ and Y211 provided measurable increases of $\mathrm{J_c(H)}$ at both 65 K and 77 K. Whether it is coincidental or not, both of these materials are known to be chemically nonreactive with 123 in thin film form; and Y211 is chemically stable in phase equilibria studies. As we suggested in an earlier publication, it is possible the requirement for chemical stability is especially important for the $<$10 nm size nanoparticle dispersions, as the particle size is so small that even slow-acting reactions might occur [7]. With chemical reaction, the superconducting/insulator interface is presumably not as sharp, which can also decrease the pinning strength of the defect [4]. Also with chemical reaction, the transition temperatures might be disturbed locally quite beyond the defect, increasing the superconducting volume fraction of insulating phase too high to allow supercurrent flow. The effect on $\mathrm{T_c}$ must be especially considered for reactive materials.

Another important factor for pinning is the lattice constant mismatch, as demonstrated for $\mathrm{CeO_2}$ additions. Because of the very large surface coverage for a small 'pseudo-layer' thickness, the $\mathrm{J_c}(H)$ properties of $\mathrm{CeO_2}$ multilayers were progressively increasing as the $\mathrm{CeO_2}$ layer coverage was decreased further [10]. It is believed the limit for reducing the $\mathrm{CeO_2}$ 'pseudo-layer' thickness was not reached yet for these studies.

For La211 and MgO additions, it appears that chemical reactions were occurring which prevented pinning improvements at 77 K. However interestingly $\mathrm{J_c}(H)$ at 65 K was increased for La211 for limited ranges of H. The lattice mismatches for La211 and MgO were also very large which could have caused unknown complications for pinning.

References

[1] P. N. Barnes, G. L. Rhoads, J. C. Tolliver, M. D. Sumption, and K. W. Schmaeman, "Compact, lightweight superconducting power generators," presented at the 12th Symp. Electromagn. Launch Technol., May 2004.

[2] D. Larbalestier, A. Gurevich, D. M. Feldmann, and A. Polyanskii, "High-$\mathrm{T_c}$ superconducting materials for electric power applications," *Nature*, vol. 414, pp. 368–377, 2001.

[3] T. Matsushita, "Flux pinning in superconducting 123 materials," *Supercond. Sci. Technol.*, vol. 13, pp. 730–737, 2000.

[4] M. Murakami, D. T. Shaw, and S. Jin, *Processing and Properties of High* $\mathrm{T_c}$ *Superconductors Volume 1, Bulk Materials*, S. Jin, Ed, NJ: World Scientific, 1993.

[5] J. L. MacManus-Driscoll, S. R. Foltyn, Q. X. Jia, H. Wang, A. Serquis, L. Civale, B. Maiorov, M. E. Hawley, M. P. Maley, and D. E. Peterson, "Strongly enhanced current densities in superconducting coated conductors of $\mathrm{YBa_2Cu_3O_{7-x}} + \mathrm{BaZrO_3}$," *Nature Mat.*, vol. 3, pp. 439–441, 2004.

[6] T. Haugan, P. N. Barnes, R. Wheeler, F. Meisenkothen, and M. Sumption, "Addition of nanoparticle dispersions to enhance flux pinning of the $\mathrm{YBa_2Cu_3O_{7-x}}$ superconductor," *Nature*, vol. 430, pp. 867–871, 2004.

[7] T. Haugan, P. N. Barnes, I. Maartense, E. J. Lee, M. Sumption, and C. B. Cobb, "Island-growth of $\mathrm{Y_2BaCuO_5}$ nanoparticles in $(211_{\sim 1.5\ \mathrm{nm}}/123_{\sim 10\ \mathrm{nm}}) \times \mathrm{N}$ composite multilayer structures to enhance flux pinning of $\mathrm{YBa_2Cu_3O_{7-\delta}}$ films," *J. Mater. Res.*, vol. 18, pp. 2618–2623, 2003.

[8] T. Haugan, P. Barnes, R. Nekkanti, J. M. Evans, L. Brunke, I. Maartense, J. P. Murphy, A. Goyal, A. Gapud, and L. Heatherly, "Deposition of $(211_{\sim 1.0\ \mathrm{nm}}/123_{\sim 10\ \mathrm{nm}}) \times \mathrm{N}$ multilayer coated conductors on Ni-based textured substrates," in *Epitaxial Growth of Functional Oxides*, Proc. Electrochem. Soc., A. Goyal, Ed., to be published.

[9] P. N. Barnes, T. J. Haugan, M. D. Sumption, S. Sathiraju, J. M. Evans, and J. C. Tolliver, "$\mathrm{YBa_2Cu_3O_{7-d}}$ films with a nanoparticulate dispersion of $\mathrm{Y_2BaCuO_5}$ for enhanced flux pinning," *Trans. MRS-J*, vol. 29, no. 4, pp. 1385–1388, 2004.

[10] P. N. Barnes, T. J. Haugan, C. V. Varanasi, and T. A. Campbell, "Flux pinning behavior of incomplete multilayered lattice structures in $\mathrm{YBa_2Cu_3O_{7-d}}$," *Appl. Phys. Lett.*, to be published.

[11] T. A. Campbell, T. J. Haugan, P. N. Barnes, I. Maartense, J. Murphy, and L. Brunke, "Flux pinning effects of $\mathrm{Y_2O_3}$ nanoparticulate dispersions in multilayered YBCO thin films," *Phys. C*, to be published.

[12] W. Wong-Ng, L. J. Swartzendruber, J. A. Kaduk, and L. H. Bennett, "Magnetic and structural properties of the "brown phase" solid solution $\mathrm{Ba(Nd_{2-x}La_x)CuO_5}$," *Phys. C*, vol. 390, pp. 213–220, 2003.

[13] T. Haugan, P. N. Barnes, L. Brunke, I. Maartense, and J. Murphy, "Effect of $\mathrm{O_2}$ partial pressure on $\mathrm{YBa_2Cu_3O_{7-x}}$ thin film growth by pulsed laser deposition," *Phys. C*, vol. 397, pp. 47–57, 2003.